Ultrafast Spin–Phonon Coupling Dynamics in $BiFeO_3$-$Bi_{0.5}K_{0.5}TiO_3$ Single Crystal

Tao Li[1,2†], Zhou Wang[2,3†], Lihua Yin[4†], Qinwen Lu[2], Yifan Ren[2,3], and Zhigao Sheng[2*]

[1]*Institutes of Physical Science and Information Technology, Anhui University, Hefei 230601, China*
[2]*High Magnetic Field Laboratory, Hefei Institutes of Physical Science, Chinese Academy of Sciences, Hefei 230031, China*
[3]*University of Science and Technology of China, Hefei 230026, China*
[4]*Key Laboratory of Materials Physics, Institute of Solid State Physics, Hefei Institutes of Physical Science, Chinese Academy of Sciences, Hefei 230031, China*

(Received 10 April 2025; accepted manuscript online 21 May 2025)

Besides equilibrium behavior, exploring the spin–phonon coupling in multiferroic materials under non-equilibrium conditions is crucial for a deep understanding of the mechanisms as well as their high-frequency applications. Here, by utilizing time-resolved reflectance spectroscopy, we demonstrate ultrafast spin–phonon coupling dynamics in multiferroic $0.58BiFeO_3$-$0.42Bi_{0.5}K_{0.5}TiO_3$ (BF-BKT) single crystals. With ultrafast laser pumping, coherent acoustic phonons with low damping are created in BF-BKT. Temperature-dependent results indicate that both the frequency and amplitude of laser-induced coherent phonons are sensitive to the emergence of antiferromagnetic order. Moreover, the spin state change driven by external magnetic fields can enhance the oscillation amplitude of the coherent acoustic phonons even above the magnetic Néel temperature. These findings experimentally confirm that spin–phonon coupling in multiferroic materials exists not only in the spin-ordered state but also in the spin-disordered state, and not only in the equilibrium state but also in the non-equilibrium state excited by ultrafast lasers, suggesting their promising applications in high-frequency devices.

DOI: 10.1088/0256-307X/42/7/070707 CSTR: 32039.14.0256-307X.42.7.070707

Multiferroic materials, which are characterized by the coexistence of magnetic and ferroelectric properties, exhibit strong interactions between their magnetic and dielectric behavior, leading to significant magnetoelectric coupling effects.[1–3] They hold great potential for many applications such as energy-efficient storage, spintronics, and sensors, as they are able to control electric polarization with a magnetic field or magnetization with an electric field.[4,5] In multiferroic materials, spin–phonon coupling (SPC) plays a key role. It can not only influence phase transitions but also enhance the strength of the magnetoelectric coupling in multiferroic materials. Moreover, the SPC is proved to be an origin of the electric order in some multiferroic materials. Accordingly, the study of SPC is crucial for understanding magnetoelectricity and other coexistence phenomena in multiferroic materials.[6–8]

To explore the SPC in multiferroic materials, several advanced techniques have been utilized, such as Raman spectroscopy, infrared spectroscopy, thermal conductivity measurement, and neutron diffraction.[8–11] For instance, Haumont *et al.* investigated the pronounced phonon anomaly near the magnetic Néel temperature (T_N) by Raman scattering, attributing it to the SPC properties of $BiFeO_3$.[9] Kamba *et al.* investigated the infrared spectrum in $SrMnO_3$ and found that the polar phonon frequency was abnormal at the antiferromagnetic (AFM) phase transition, confirming the existence of strong SPC.[12] Petit *et al.* found the gap opening in the lower part of the T_N in the dispersion of transverse acoustic phonon modes along the lower part of the ferroelectric axis in $YMnO_3$ using inelastic neutron scattering.[8] Most of these studies explore the SPC from the perspective of equilibrium or quasi-equilibrium states, but very few activities have been undertaken for SPC in multiferroic materials under non-equilibrium, although it is crucial for a deeper understanding of its mechanism and the high-frequency applications of multiferroic materials.

A powerful tool to detect the dynamic states in a material is ultrafast optical spectroscopy. With the development of ultrafast femtosecond lasers, this technique has been widely used in dynamic studies, including ultrafast carrier dynamics, control of metastable phase transitions, ultrafast manipulation of magnetization, coherent phonons in solids, and light-induced superconducting states.[13–16] Among them, ultrafast coherent phonon techniques, which involve the generation and manipulation of coherent lattice vibrations (phonons), may provide a unique and powerful approach for studying SPC because they allow for the direct observation of the dynamic interactions between spins and lattice vibrations with femtosecond resolution.[17–20] This is of great importance for the study of SPC in multiferroic materials.

†These authors contributed equally to this work.
*Corresponding author. Email: zhigaosheng@hmfl.ac.cn
© 2025 Chinese Physical Society and IOP Publishing Ltd. All rights, including for text and data mining, AI training, and similar technologies, are reserved.

In this work, we explored the ultrafast spin–phonon dynamics of the multiferroic antiferromagnet $0.58BiFeO_3$-$0.42Bi_{0.5}K_{0.5}TiO_3$ (BF-BKT) single crystals via time-resolved reflectance spectroscopy. After ultrafast laser pumping, the coherent acoustic phonon (CAP) with a frequency of 28.3 GHz is created in BF-BKT. Within such a laser pumping-induced non-equilibrium state, the temperature-dependent results illustrate that both the frequency and oscillation amplitude of the coherent phonon are sensitive to the emergence of AFM order. Additional magnetic field-dependent results indicate that the spin state change driven by the magnetic field can efficiently enhance the oscillation amplitude of CAP.

The multiferroic BF-BKT single crystals studied in this work were grown by the self-flux method. K_2CO_3 and Bi_2O_3 in an appropriate ratio were used as the flux. The stoichiometric materials K_2CO_3, Fe_2O_3, TiO_2, and Bi_2O_3 were mixed with the flux in a suitable ratio. The resulting mixture was placed into a platinum crucible, heated to 1200 °C, and soaked at 1200 °C for 5 h. The mixture was slowly cooled to 950 °C at a rate of 3 °C/h, and then the furnace was turned off. It has been reported that by compounding with $Bi_{0.5}K_{0.5}TiO_3$, the magnetoelectric coupling coefficient of $BiFeO_3$ can be improved. BF-BKT studied here possesses a relatively high magnetoelectric coupling coefficient of $\alpha_{ME} = 0.61$ mV/cm.[21]

BF-BKT tetragonal crystal structure with the space group $P4mm$ is shown in Fig. 1(a). The A-sites of the BF-BKT lattice are occupied by Bi or K ions. In addition, the B-site ions are occupied by Fe or Ti ions, forming FeO_6 or TiO_6 oxygen octahedrons. The K ions are placed in the Bi sublattice, and the Ti ions partly occupy the Fe sublattice of the $BiFeO_3$ structure.[22] The adjacent irons in BF-BKT are configured with antiparallel spins, and the magnetism is mainly due to the strong AFM superexchange between adjacent irons. The result of the X-ray diffraction (XRD) measurement of BF-BKT single crystal is shown in Fig. 1(b). It only displays the (0 0 l) Bragg peaks ($l = 1, 2, 3$), without any other peaks, indicating the high-quality single crystallinity of the sample. The lateral dimensions of BF-BKT single crystal are 1 mm × 0.6 mm with a thickness of 0.5 mm, and its optical image is shown in the inset of Fig. 1(b).

The magnetization properties of BF-BKT single crystals were investigated using a superconducting quantum interference device (SQUID) magnetometer. Figure 1(c) shows the temperature-dependent magnetization (M–T) curves under the zero-field-cooling (ZFC) and field-cooling (FC) along the out-of-plane [001] axis at a magnetic field of $\mu_0 H = 100$ Oe. The magnetization decreases with increasing temperature, and the magnetization change accelerates linearly at $T > 255$ K. It indicates an AFM transition associated with a kink in both the ZFC and FC curves occurs at $T \sim 255$ K. The isothermal magnetic hysteresis loops (M–H) curves obtained at different temperatures with magnetic field along the out-of-plane [001] axis are shown in Fig. 1(d). At low temperatures ($T < T_N$), it exhibits obvious nonlinear behavior with zero remanence. The first derivative of magnetization and magnetic field [dM/dH, shown in the inset of Fig. 1(d)] possesses a significant transition at $\mu_0 H = 1.7$ T when the temperature is 250 K, which indicates a spin state modulation driven by magnetic field. While the linear M–H curves and negligible change of dM/dH reveal the typical paramagnetic (PM) characteristics at $T > T_N$.

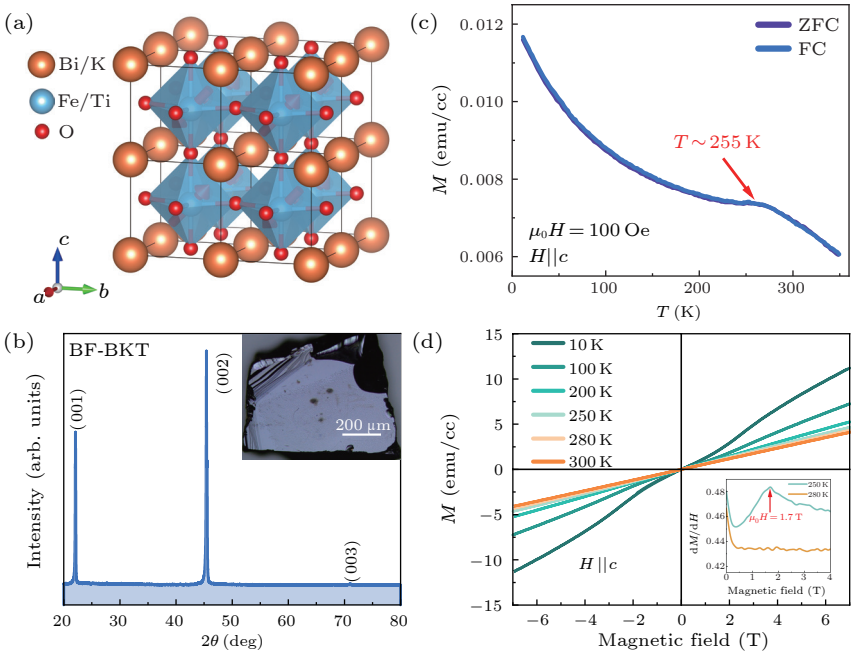

Fig. 1. (a) A crystal structure diagram of BF-BKT with magnetic moments (red arrows). (b) The XRD pattern for a natural facet of BF-BKT single crystal. Inset in (b) is the optical image of the single crystal. (c) Temperature dependence of magnetization measured with zero-field cooling (ZFC, purple line) and field cooling (FC, blue line) with $\mu_0 H = 100$ Oe along the [001] axis. (d) Hysteresis loops measured at different temperatures along the [001] axis. Inset in (d) is the corresponding derivatives of M–H curves at 250 K and 280 K, plotted as a function of magnetic field.

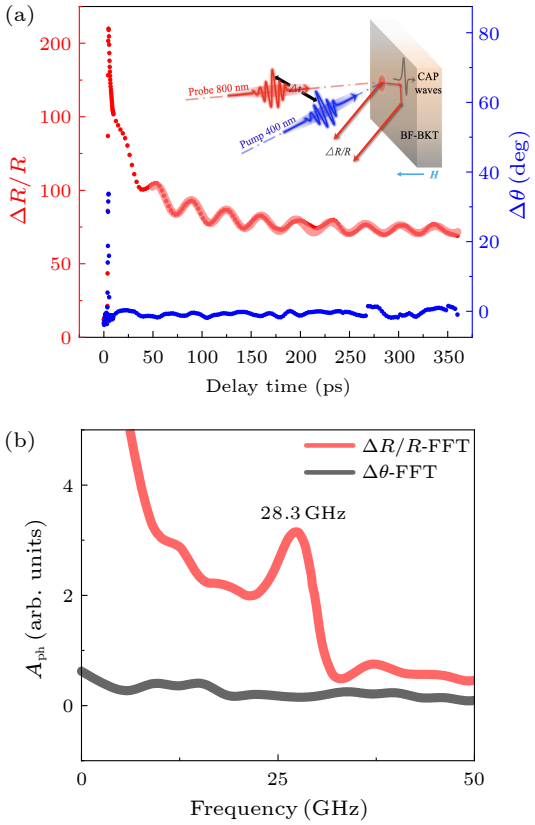

Fig. 2. (a) Time-resolved $\Delta R/R$ (red) measured at 300 K and $\Delta\theta$ (blue) measured at 10 K of a [001] BF-BKT single crystal. The red solid line is the fitting of the data using Eq. (1). Inset is the sketch of the two-color pump-probe experiment setup. (b) The FFT of experimental $\Delta R/R$ and $\Delta\theta$ data.

In order to explore the phonon dynamics in BF-BKT, the time-resolved reflectance spectroscopic measurements have been done, and the typical results obtained at 300 K are shown in Fig. 2. First, the absorption spectra of BF-BKT were measured, and the results are shown in Fig. S2(a) of the Supplementary Materials (SM). It is found that BF-BKT crystal has strong absorption at 400 nm, while weak absorption at 800 nm. The experimental setup is shown in the inset of Fig. 2(a). The experiment uses a regeneratively amplified Ti:sapphire laser system with a pulse of 100 fs and a repetition rate of 1 kHz. The system delivers a 400 nm (3.1 eV) pump at 4.8 mJ/cm^2 and an 800 nm (1.55 eV) probe at 0.1 mJ/cm^2 on the sample. The sample is focused at an incidence of nearly 45 degrees and cross-polarized linearly to suppress the background signal caused by pump light. The time delay between pump and probe pulses was precisely controlled by a linear translational stage. The reflectivity change ($\Delta R/R$) is given as a function of the pump-probe time delay at 300 K. The optically pumped thermal expansion leads to the generation of strain pulses; then, interference occurs between the probe light reflected from the free surface and the wavefront of the propagating strain pulse, resulting in coherent oscillations of the reflected light.[23–25]

Figure 2(a) shows the initial excitation of hot carriers when the pump and probe pulse lasers coincide in time and space on the sample surface, followed by a periodic oscillation signal in the process of exponential decay of thermal diffusion. Owing to the relaxation of hot charge carriers through the lattice, the $\Delta R/R$ exhibits a large exponential decay background. The accompanying oscillation signal is attributed to the CAP excitation in the sample, which is considered to be a coherent longitudinal acoustic (LA) phonon mode.[26] Via fast Fourier transformation (FFT) analysis, the phonon frequency is obtained as 28.3 GHz, as shown in Fig. 2(b). Furthermore, as shown in Fig. S2(b) of SM, there is negligible oscillation signal (CAP) that can be found when the pump 800 nm/probe 800 nm configuration is utilized. This feature agrees with the fact that the BF-BKT has quite small optical absorption at 800 nm.

The propagation of strain pulses generated by transient thermal stress was first proposed by Thomsen *et al.*[27] Strain waves induced by electronic and thermal stresses can tune the local dielectric constant, leading to discontinuities in reflectivity, which are frequently observed in high-quality crystalline $BiFeO_3$ samples.[27] The equilibrium point of the lattice is broken, which causes the crystal to deform after a certain time, i.e., to emit acoustic phonons. The relative displacement of the atoms in the crystal leads to a strain field $E(z,t)$, which causes a spatio-temporal change in the refractive index. The transient reflectivity signal can be mathematically approximated by a summation of the exponential decay function and an attenuating oscillation function,

$$\frac{\Delta R}{R} = a_0 + b\exp\left(-\frac{t}{\tau_0}\right) + c\sin(2\pi f t+\varphi)\exp\left(-\frac{t}{\tau_1}\right), \quad (1)$$

where b and τ_0 are the amplitude and relaxation time for hot carrier excitation corresponding to the large decay background in the signal. c, f, φ, and τ_1 present the amplitude, frequency, initial phase, and damping time of the LA phonon mode, respectively. α is used to describe the damping factor of coherent oscillation. The fitting results are plotted in Fig. 2(a) as a red solid line curve, which all well match the measurement data. It is found that laser-induced coherent phonon in BF-BKT has a relatively low damping factor of $\alpha \sim 0.0102$. CAP loses less energy during propagation, maintaining its coherent properties and continuous oscillation for a long time in BF-BKT. Due to the slow energy loss, we can more clearly observe and analyze the CAP state (frequency, amplitude, etc.) under external stimulation (magnetic field or temperature).

The ultrafast CAP dynamics measured at different temperatures without a magnetic field are shown in Fig. 3(a). With the increase of temperature from 10 to 280 K, the laser-induced coherent phonon presents some changes, especially near T_N. We fitted these experimental data of BF-BKT single crystal using the above Eq. (1) to quantitatively describe the phenomenon of coherent oscillation. The obtained frequency and amplitude at different

temperatures are collected in Figs. 3(b) and 3(c), respectively. It shows that with the increase of temperature, the frequency of the laser-induced coherent phonon (f_{ph}) decreases almost linearly from 29.8 GHz at 10 K to 28.3 GHz at 280 K. As for the amplitude of coherent phonon oscillation (A_{ph}), the temperature dependence is different. As shown in Fig. 3(c), the A_{ph} is only ∼1.9 at 10 K, and it remains almost constant below 200 K. While it starts to increase sharply when the ambient temperature is close to T_N. As the temperature rises to 280 K, the A_{ph} is enhanced up to ∼3.4 with a relative change of ∼80%. The rapid change of the A_{ph} value near T_N indicates that the dynamic behavior of coherent phonons is tightly related to the spin state of multiferroic BF-BKT, that is, ultrafast SPC dynamics.

As a typical multiferroic material, the spin state of BF-BKT crystal can be effectively regulated not only by temperature but also by the application of an external magnetic field. This method is particularly convenient for device applications. Time-resolved reflectance spectroscopic measurements under applied magnetic fields have been conducted. It was found that a 7 T magnetic field has a negligible effect on the frequency of ultrafast coherent phonons, but it significantly increases the amplitude of ultrafast coherent phonons. As shown in Fig. 3(c), the A_{ph} is enhanced from 1.9 to 2.4 at 10 K when the magnetic field changes from 0 to 7 T. Such magnetic field-induced A_{ph} enhancement persists across the entire measurement temperature range.

In order to further explore ultrafast SPC dynamics, the detailed magnetic field effects in different temperature regions have been carefully examined. Figure 4(a) displays the typical time-resolved $\Delta R/R$ data measured with different magnetic fields from 0 to 7 T at 250 K. It shows that the magnetic field has a negligible effect on the frequency of ultrafast coherent phonons, but it can significantly enhance the amplitude of ultrafast coherent phonons, as mentioned above. The magnetic field dependences of the A_{ph} obtained at 100 and 250 K are summarized in Fig. 4(b). It shows that under low magnetic fields ($\mu_0 H < 1$ T), the A_{ph} remains nearly constant, indicating that BF-BKT single crystal is in a stable AFM state. When the magnetic field increases to more than 1.7 T, the A_{ph} increases dramatically. At 250 K, when the magnetic field is increased from 1.7 to 3 T, the A_{ph} can be enhanced from 3.0 to 3.9, with a relative change of ∼30.17%. With further increasing of the magnetic field, the A_{ph} increases slowly and reaches 4.1 at 6 T. The magnetic field-dependent behavior of A_{ph} obtained at 100 K is similar to that of 250 K, except that the critical magnetic field is enhanced to 2.4 T.

In the AFM state of BF-BKT, the net magnetic moment is zero. When a magnetic field is applied, the Fe^{3+} ions in BF-BKT reorient their spins, leading to a loosening of spins, which in turn enhances the interaction strength between spins and the lattice.[28,29] Figure 4(c) displays the first derivatives of the M–H curves (dM/dH) as a function of magnetic field. It is interesting to find that the spin-reorientation field H_{SR} is 1.7 T and 2.4 T for $T = 250$ K and 100 K, respectively, which are exactly the same as the critical fields for the A_{ph} enhancement, as shown in Fig. 4(b). The coincidence of the critical magnetic fields of the magnetically controlled A_{ph} and the spin-reorientation fields H_{SR} once again proves the strong SPC in BF-BKT, and it persists even in the ultrafast laser excited non-equilibrium state.

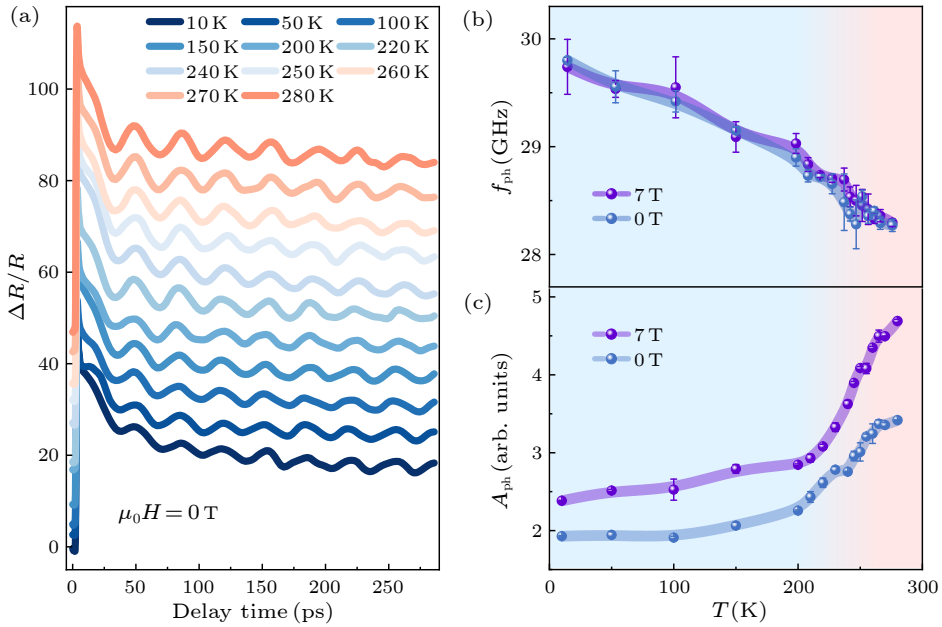

Fig. 3. (a) Time-resolved $\Delta R/R$ measured at different temperatures from 10 to 280 K with a pump fluence of 4.8 mJ/cm^2. Temperature-dependent damped oscillation frequency (b) and amplitude (c) of laser-induced coherent phonon measured with magnetic fields of 0 and 7 T.

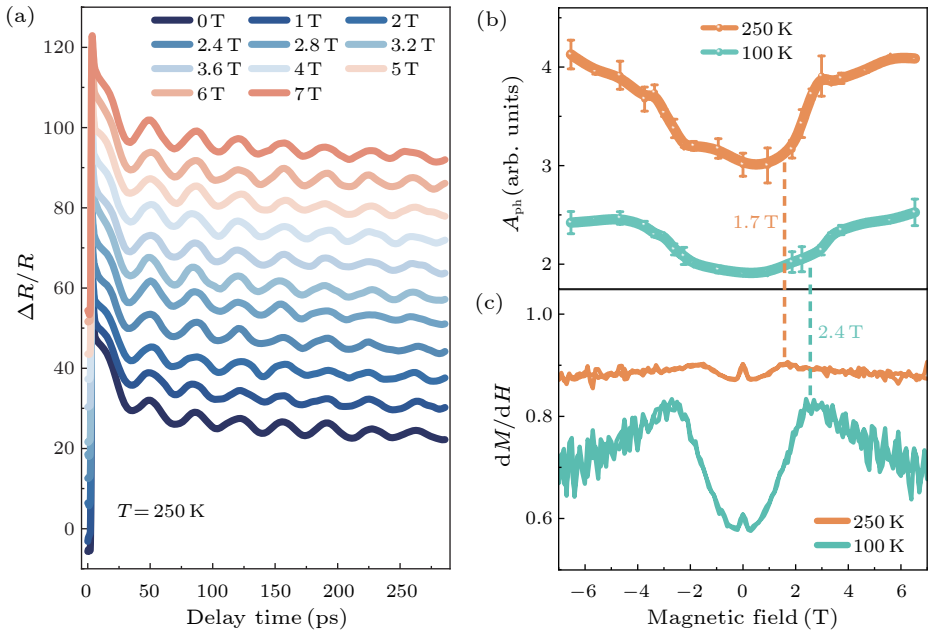

Fig. 4. (a) Time-resolved $\Delta R/R$ measured with different magnetic fields from 0 to 7 T at 250 K with a pump fluence of 4.8 mJ/cm^2. (b) The damped oscillation amplitude obtained from Eq. (1), plotted as a function of magnetic field. (c) Corresponding derivatives of M–H curves (dM/dH) at different temperatures along the [001] axis.

In the aforementioned studies on the effects of temperature and magnetic fields, time-resolved $\Delta R/R$ experiments provide insights into the dynamic behavior of phonons. Another possible effect in such non-equilibrium states induced by ultrafast laser excitation is the laser-induced change in spin state, in addition to triggering coherent phonons. The interplay between light field regulation of spin state and temperature/magnetic field effects would complicate the analysis. To address this issue, time-resolved Kerr spectroscopic measurements were also conducted, with typical results at 10 K shown by the blue curve in Fig. 2(a). In addition, FFT analysis of the $\Delta\theta$ curve reveals no obvious frequency peaks, which is close to system noise. The weak oscillations in the $\Delta\theta$ curve are caused by system errors. It shows that the ultrafast laser pump used here does not alter the original AFM spin structure. Consequently, it is clarified that the observed temperature/magnetic field effects do not include spin state influences induced by laser pumping.

Let us turn back to the temperature and magnetic field effects, and there are two additional points worth noting. First, compared to the low temperature (∼100 K) case, although the change in spin orientation caused by the magnetic field at 250 K is relatively small [Fig. 4(c)], the corresponding magnetic enhancement of A_{ph} is much larger [Fig. 4(b)]. This feature can also be found in the temperature-dependent behaviors shown in Fig. 3(c), implying that the SPC near the magnetic transition temperature (T_N) is more easily modulated by temperature and magnetic field. It has been reported that the magnetic exchange interaction energy is suppressed to promote the volume expansion near the T_N, and it shows that the elastic energy is completely released, resulting in a sudden jump of the space lattice.[30–33] Second, the magnetic field also increases A_{ph} even above T_N [Fig. 3(c)]. This phenomenon indicates that SPC can exist over a wide temperature range, even before the spin-ordered structure is fully established, owing to the strong short-range spin order.[34] Above T_N, the spin-lattice coupling does not disappear, leading to the fact that the A_{ph} of CAP is still modulated by the magnetic field. This feature not only benefits the further understanding of SPC in multiferroic materials but also enhances the magnetic control effect, especially in the operating temperature range of subsequent magnetic control devices.

In summary, the ultrafast SPC dynamics in multiferroic BF-BKT single crystals have been studied carefully by using time-resolved reflectance spectroscopy with variations in both temperature and magnetic field. The ultrafast laser pumping can produce CAP in BF-BKT with a frequency of 28.3 GHz and a low damping factor of 0.0102. The temperature and magnetic field dependence indicates that the frequency and amplitude of laser-induced coherent phonons are tightly related to the emergence of the AFM spin state and its magnetic field regulation. These results confirm that robust SPC persists in multiferroic materials even under non-equilibrium conditions induced by ultrafast laser excitation, suggesting their potential application in high-frequency devices.

The data that support the findings of this study are available from the corresponding author upon reasonable request.

Acknowledgements. This work was supported by the National Key R&D Program of China (Grant No. 2021YFA1600200), the National Natural Science Foundation of China (Grant Nos. U2032218 and 12111530283). A portion of this work was performed on the Steady High Magnetic Field Facilities, Chinese Academy of Science and

supported by the High Magnetic Field Laboratory of Anhui Province.

References

[1] Fiebig M, Lottermoser T, Meier D, and Trassin M 2016 *Nat. Rev. Mater.* **1** 16046
[2] Schmid H 1994 *Ferroelectrics* **162** 317
[3] Vaz C A F, Hoffman J, Ahn C H, and Ramesh R 2010 *Adv. Mater.* **22** 2900
[4] Spaldin N A and Ramesh R 2019 *Nat. Mater.* **18** 203
[5] Gong Y F, Wu P, Liu W F, Wang S Y, Liu G Y, and Rao G H 2012 *Chin. Phys. Lett.* **29** 047701
[6] Rawat R, Phase D M, and Choudhary R J 2017 *J. Magn. Magn. Mater.* **441** 398
[7] Katoch R, Sekhar C D, Adyam V, Scott J F, Gupta R, and Garg A 2016 *J. Phys. Condens. Matter* **28** 075901
[8] Petit S, Moussa F, Hennion M, Pailhès S, Pinsard-Gaudart L, and Ivanov A 2007 *Phys. Rev. Lett.* **99** 266604
[9] Haumont R, Kreisel J, Bouvier P, and Hippert F 2006 *Phys. Rev. B* **73** 132101
[10] Singh M K and Katiyar R S 2011 *J. Appl. Phys.* **109** 07D916
[11] Xu X, Wang X, Chang P, Chen X, Guan L and Tao J 2022 *J. Phys. Chem. C* **126** 10574
[12] Kamba S, Goian V, Skoromets V, Hejtmánek J, Bovtun V, Kempa M, Borodavka F, Vaněk P, Belik A A, Lee J H, Pacherová O, and Rabe K M 2014 *Phys. Rev. B* **89** 064308
[13] Breusing M, Ropers C and Elsaesser T 2009 *Phys. Rev. Lett.* **102** 086809
[14] Padmanabhan P, Buessen F L, Tutchton R, Kwock K W C, Gilinsky S, Lee M C, McGuire M A, Singamaneni S R, Yarotski D A, Paramekanti A, Zhu J X, and Prasankumar R P 2022 *Nat. Commun.* **13** 4473
[15] Sun F, Yang M, Yang M W, Wu Q, Zhao H, Ye X, Shi Y, and Zhao J 2018 *Chin. Phys. Lett.* **35** 116301
[16] Lee M C, Kim C H, Kwak I, Seo C W, Sohn C, Nakamura F, Sow C, Maeno Y, Kim E A, Noh T W, and Kim K W 2019 *Phys. Rev. B* **99** 144306
[17] Yee K J, Lee K G, Oh E, Kim D S, and Lim Y S 2002 *Phys. Rev. Lett.* **88** 105501
[18] Martinez L M, Liu Y, Petrovic C, Haldar S, Griepe T, Atxitia U, Campbell M, Pettes M, Prasankumar R P, Santos E J G, Singamaneni S R, and Padmanabhan P 2023 arXiv:2308.14931 [cond-mat.mtrl-sci]
[19] Hu L L, Yang M, Wu Y L, Wu Q, Zhao H, Sun F, Wang W, He R, He S L, Zhang H, Huang R J, Li L F, Shi Y G, and Zhao J 2019 *Phys. Rev. B* **99** 094307
[20] Lee M C, Kim C H, Kwak I, Seo C W, Sohn C, Nakamura F, Sow C, Maeno Y, Kim E A, Noh T W, and Kim K W 2019 *Phys. Rev. B* **99** 144306
[21] Yin L H, Zhao G, Tong P, Yang J, Zhu X, Song W, and Sun Y 2023 *Acta Mater.* **255** 119044
[22] Sando D, Barthélémy A, and Bibes M 2014 *J. Phys. Condens. Matter* **26** 473201
[23] Lobad A I and Taylor A J 2001 *Phys. Rev. B* **64** 180301
[24] Ruello P and Gusev V E 2015 *Ultrasonics* **56** 21
[25] Kuznetsov A V and Stanton C J 1994 *Phys. Rev. Lett.* **73** 3243
[26] Ruello P, Pezeril T, Avanesyan S, Vaudel G, Gusev V, Infante I C, and Dkhil B 2012 *Appl. Phys. Lett.* **100** 212906
[27] Thomsen C, Grahn H T, Maris H J, and Tauc J 1986 *Phys. Rev. B* **34** 4129
[28] Magill B A, Thapa S, Holleman J, McGill S, Munekata H, Stanton C J, and Khodaparast G A 2020 *Phys. Rev. B* **102** 045306
[29] Padmanabhan H, Poore M, Kim P K, Koocher N Z, Stoica V A, Puggioni D, Wang H, Shen X, Reid A H, Gu M, Wetherington M, Lee S H, Schaller R D, Mao Z, Lindenberg A M, Wang X, Rondinelli J M, Averitt R D, and Gopalan V 2022 *Nat. Commun.* **13** 1929
[30] Talbayev D, Lee J, Trugman S A, Zhang C L, Cheong S W, Averitt R D, Taylor A J, and Prasankumar R P 2015 *Phys. Rev. B* **91** 064420
[31] Xu Z, Deng B, Hu S, and Chen L 2020 *Appl. Phys. Lett.* **117** 122901
[32] Jang K J, Lim J, Ahn J, Kim J H, Yee K J, Ahn J S, and Cheong S W 2010 *New J. Phys.* **12** 023017
[33] Lim D, Averitt R D, Demsar J, Taylor A J, Hur N, and Cheong S W 2003 *Appl. Phys. Lett.* **83** 4800
[34] Li G, Ma S, Li Z, Zhang Y, Diao J, Xia L, Zhang Z, and Huang Y 2022 *ACS Nano* **16** 7861